Supporting information

Inter-layer bismuthene as a charge-transporter improves photoelectrochemical water oxidation activity of bismuth vanadate-metal-organic framework

Deepak Kumar,[a] Sagnik Mukherjee,[a] Arindam Indra[a*]

[a]*Department of Chemistry, Indian Institute of Technology (BHU), Varanasi, UP-221005, India*

E-mail: arindam.chy@iitbhu.ac.in

Chemicals

Bismuth nitrate pentahydrate, dimethyl formamide (DMF), potassium iodide, dimethyl sulfoxide (DMSO), sodium hydroxide, sodium borohydride, sodium dihydrogen phosphate, disodium hydrogen phosphate, isopropanol, and chloranilic acid were procured from MERCK Life Sciences Pvt. Ltd., India. Vanadyl acetylacetonate was purchased from SRL Pvt. Ltd., India. Nickel chloride hexahydrate, was purchased from SD Fine Pvt. Ltd., India. *Para*-benzoquinone was purchased from Loba Chemie Pvt. Ltd., India, and Ethanol (99%) was procured from Chengdu, China. Fluorine-doped tin oxide (FTO, 1x2 cm^{-2}, resistivity ~7Ω/sq) was purchased from Sigma. Double-distilled water was utilized for washing, synthesis, and electrochemical measurements. The chemicals were used as received without further purification.

Instruments

Rigaku Smart Lab 9 kW Powder X-ray diffractometer with Cu-K_α (λ = 1.5418 Å) radiation was used for PXRD measurements in the $5° < 2\theta < 90°$ range.

Scanning electron microscopy (SEM) was recorded on EVO-Scanning Electron Microscope MA15/18 from CARL ZEISS MICROSCOPY LTD. Energy-dispersive X-ray (EDX) and elemental mapping analysis were performed in Oxford Instruments Nanoanalysis (51N1000). Transmission electron microscopic (TEM) studies were performed in Tecnai G2 F30 TWIN from FEI Company of USA (SEA) PTE, LTD. A piece of the photoanode@FTO was sonicated in 2 mL ethanol for 10 minutes and drop cast on a Cu grid for TEM measurements.

Raman spectroscopy was carried out on an alpha 300 confocal Raman microscope (WITec, Germany) with a spectral resolution of ~1 cm^{-1}. A 785 nm laser served as the excitation source, operated at 1–2 mW on the sample surface to minimize thermal effects, with an acquisition time of 10 s.

Solid-state UV-vis reflectance spectroscopy was performed using a UV-2600 spectrophotometer (Shimadzu; Japan) from 200 to 800 nm. Photoluminescence spectra were acquired with a Fluorolog FL-3-11 by Horiba Jobin-Yvon.

X-ray photoelectron spectroscopy (XPS) was performed using a K_α Thermo Fisher Scientific X-ray photoelectron spectrometer. Origin 8.5 software was used to analyze the XPS data.

A Metrohm Autolab M204 electrochemical workstation was used to perform the photoelectrochemical and electrochemical measurements.

Experimental

Fabrication of the photoanode $BiVO_4$@FTO[1]

2.3 mmol *para*-benzoquinone was taken in 10 mL ethanol and stirred for 30 minutes. 0.01 mol of potassium iodide was added to 25 mL of double-distilled water to prepare a solution. 1.0 mmol bismuth nitrate pentahydrate was added to potassium iodide solution and stirred for 10 minutes, followed by the addition of *para*-benzoquinone solution and stirred for 15 minutes. The brownish-red color of bismuth oxyiodide (BiOI) was formed. The pH of the solution was maintained below 2 by the addition of nitric acid. For the electrodeposition of BiOI, FTO was used as the working electrode, Ag/AgCl as the reference electrode, and Pt wire as the counter electrode. A cathodic potential of -0.2 V *vs.* Ag/AgCl electrode was applied for 120 seconds to get a uniform film of BiOI on FTO. The

BiOI film was dried for 1 hour at 60 °C in an air oven. Next, the BiOI on FTO film was dipped in a 0.2 M solution of vanadyl acetylacetonate in dimethyl sulfoxide and taken out immediately. The film was calcined at 450 °C (ramp rate of 2 °C/minute) in a tubular furnace followed by natural cooling. The yellow-greenish films on FTO were soaked in 1.0 M NaOH solution for 15 minutes to remove the vanadium pentoxide formed during calcination. After washing with distilled water and drying, the yellow-colored bismuth vanadate film on FTO was obtained.[1]

Synthesis of bismuthene[2]

In a round-bottom flask, 0.5 mmol bismuth nitrate pentahydrate was dissolved in 15 mL ethylene glycol by sonication to get a transparent solution. The solution was purged with argon (Ar) gas and stirred for 30 minutes at 120 °C. The solution was kept at room temperature in an argon atmosphere. In 5 mL of water, 20 mmol of sodium borohydride was dissolved in an Ar atmosphere and dropwise added to the Bi^{3+} solution using a syringe. A black precipitate appeared, and after the addition of the whole sodium borohydride solution (10 minutes), the black precipitate was immediately collected through centrifugation (10,000 RPM, 5 minutes). The solid was washed with ethanol three times and kept under vacuum for drying at room temperature.[2]

Synthesis of nickel chloranilic acid MOF (Ni-MOF)

0.1 mmol chloranilic acid (in 5 mL DMF) was added to 0.1 mmol nickel chloride hexahydrate (in 5 mL DMF) and sonicated for 10 minutes. The suspension was transferred to a Teflon cup and solvothermally treated at 120 °C for 6 hours. The MOF was collected via centrifugation (8000 RPM, 5 minutes), washed with water (3 times) and ethanol (2 times), and dried in an oven at 60 °C overnight.[3]

Photoanode fabrication

(i) 10 mg bismuthene was dispersed in 10 mL of ethanol by sonication for 15 minutes. $BiVO_4$@FTO was immersed in bismuthene dispersion for 5 minutes and dried in a vacuum to get $BiVO_4$/Bi.

(ii) 5 mg of Ni-MOF was dispersed in 10 mL of ethanol by sonication for 15 minutes. The $BiVO_4$/Bi photoanode was immersed in a mixture for 5 minutes and dried in a vacuum to obtain $BiVO_4$/Bi/Ni-MOF. The photoanodes were kept in a vacuum for drying.

Similarly, other photoanodes were prepared as shown in Table S1.

Table S1. Modified photoanodes used for the PEC water splitting.

No.	Catalyst system	Catalyst name
1.	$BiVO_4$	$BiVO_4$
2.	Bismuthene	Bi
3.	Nickel-chloranilate framework	Ni-MOF
4.	$BiVO_4$/Bismuthene	$BiVO_4$/Bi
5.	$BiVO_4$/Nickel-chloranilate framework	$BiVO_4$/Ni-MOF
6.	$BiVO_4$/Bismuthene/Nickel-chloranilate framework	$BiVO_4$/Bi/Ni-MOF

Photoelectrochemical and electrochemical measurements

All electrochemical measurements were carried out in a single-compartment photoelectrolytic cell having 25 mL electrolyte (0.5 M phosphate buffer solution with pH 7) with the photoanode@FTO as the working electrode, Ag/AgCl as the reference electrode, and Pt wire as the counter electrode. A Metrohm Autolab M204 electrochemical workstation was used to perform the photoelectrochemical measurements. Visible light (Orient Electric) was used for PEC measurements. All potentials were converted to the reversible hydrogen electrode (RHE) using the following equation:

$$\mathbf{E_{(RHE)} = E_{(Ag/AgCl)} + 0.0591pH + 0.197}$$

Chopped light current-time (i-t) curves were recorded with an alternating light on/off irradiation at every 30s with an applied potential of 1.23 V vs. RHE.

Electrochemical impedance spectroscopic (EIS) measurements were carried out in the frequency range of 0.001 to 100,000 Hz with an amplitude of 20 mV in the dark and light. The charge transfer resistance (R_{ct}) was calculated based on the semicircle diameter observed in the Nyquist plots.

Mott-Schottky (M-S) plots were recorded over an AC frequency of 0.5 kHz, 1.0 kHz, and 1.5 kHz in the dark with the applied bias ranging from -0.28 to 1.5 V vs. RHE.

The applied bias photon-to-current efficiency (ABPE) was calculated according to the equation:

$$\mathbf{ABPE(\%) = \frac{(1.23-V)\times J}{P} \times 100\%}$$

Where J is the photocurrent density (mA cm^{-2}), V is the applied bias (V *vs.* RHE), and P is the incident light density (100 mW cm^{-2}).

The incident photon-to-current conversion efficiency (IPCE) was performed under monochromatic irradiation from a Xe lamp at 1.23 V *vs.* RHE according to the following equation:

$$\mathbf{IPCE(\%) = \frac{1240\,x\,J(\lambda)}{P(\lambda)\,\lambda} \times 100\%}$$

Where $J(\lambda)$, λ, and $P(\lambda)$ are photocurrent density (mA cm^{-2}), wavelength of light (nm), and power density of monochromatic light (mW cm^{-2}), respectively.[1]

Figures

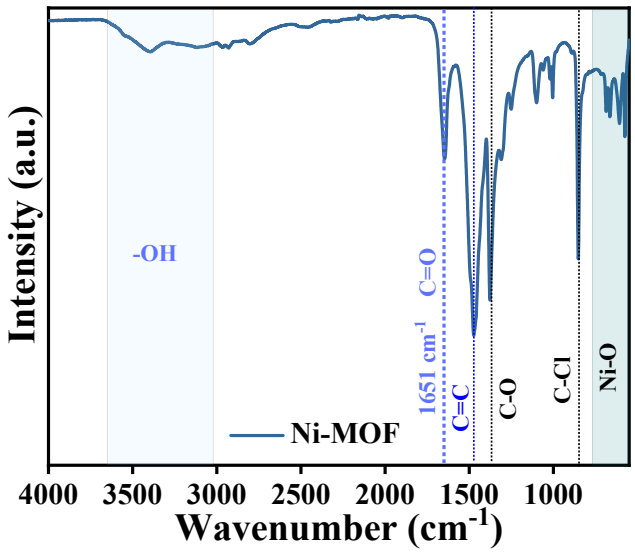

Figure S1. The attenuated total reflection Fourier-transformed infrared (ATR-FTIR) spectrum of Ni-MOF[3] showing characteristic peaks: broad O–H stretching at 3500–3200 cm^{-1}, quinone C=O stretch at 1651 cm^{-1}, aromatic C=C stretches at 1600–1500 cm^{-1}, C–O stretches at 1400–1200 cm^{-1}, aromatic ring vibrations at 1200–1000 cm^{-1}, C–Cl stretching at 850 cm^{-1}, and Ni─O vibrations at 500–800 cm^{-1}. Aromatic C–H stretching appears near 3100–3000 cm^{-1}.

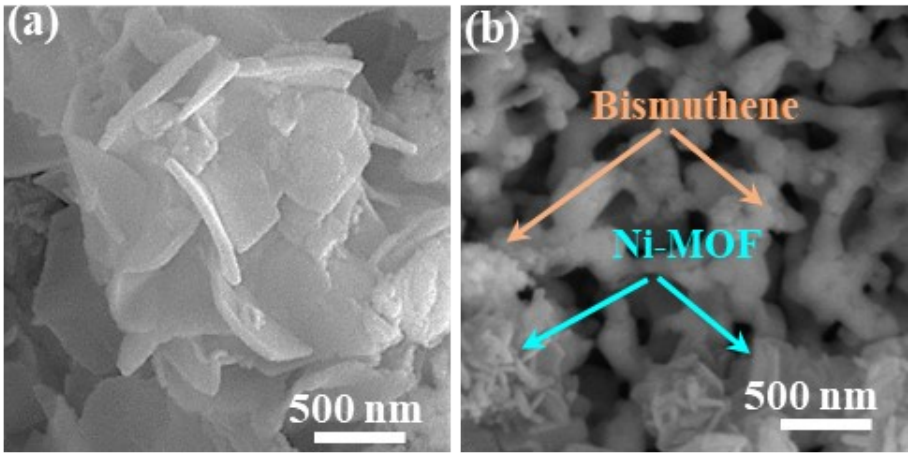

Figure S2. Scanning electron microscope (SEM) images of the photoanodes: (a) Ni-MOF, (b) $BiVO_4$/Bi/Ni-MOF.

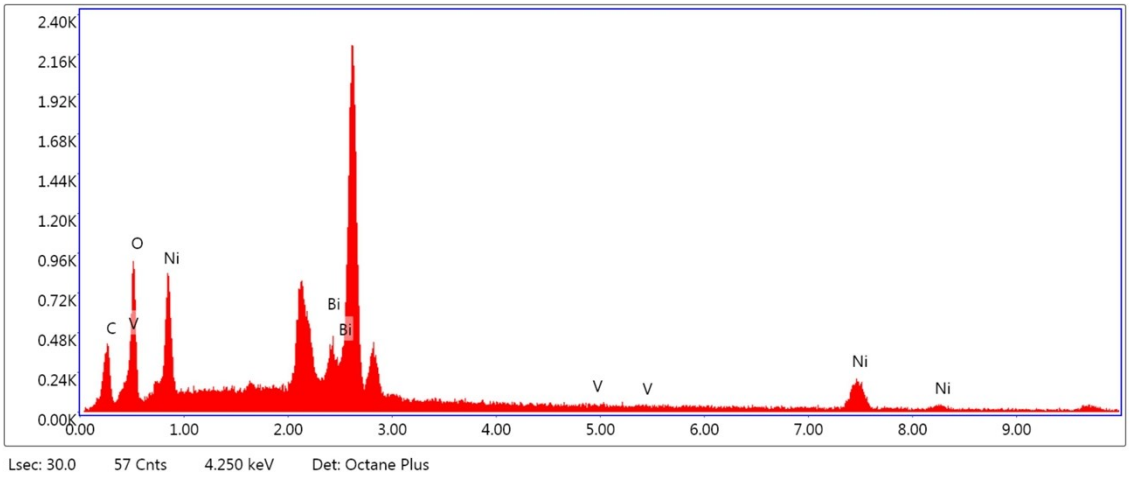

Figure S3. Energy dispersive X-ray spectrum of $BiVO_4$/Bi/Ni-MOF showing the presence of elements Bi, V, Ni, and O.

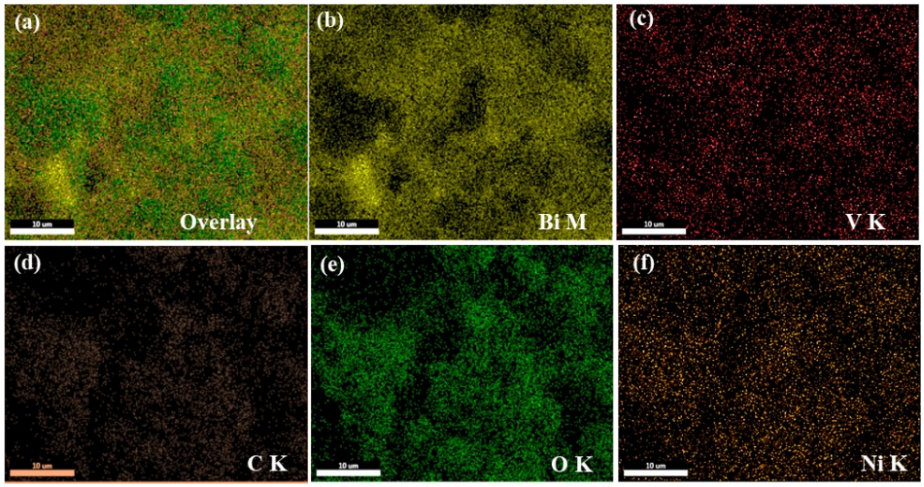

Figure S4. Elemental mapping of $BiVO_4$/Bi/Ni-MOF showing the presence of elements Bi, V, Ni, O, and C (scale: 10 μm).

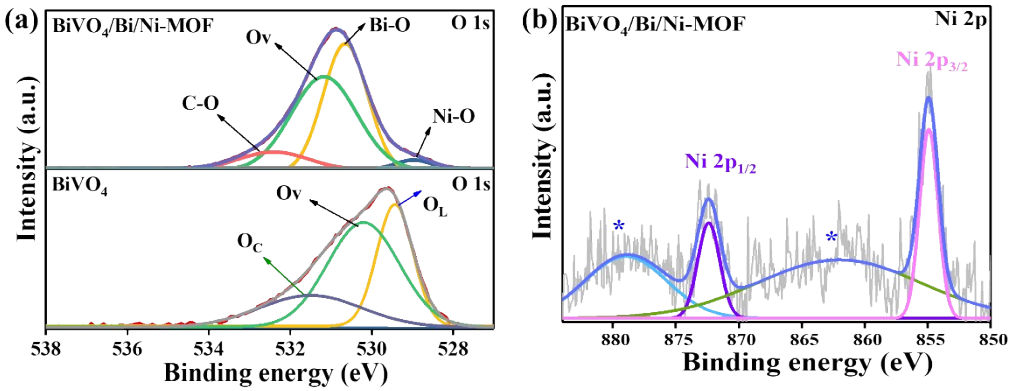

Figure S5. X-ray photoelectron spectra of $BiVO_4$ compared with $BiVO_4$/Bi/Ni-MOF. (a) O 1s spectrum, The O 1s XPS of $BiVO_4$ was fitted into three peaks. The XPS of $BiVO_4$/Bi/Ni-MOF were fitted into three peaks for Ni–O, Bi–O, oxygen vacancy (O_v), and –CO groups,[4] (b) Ni 2p XPS of $BiVO_4$/Bi/Ni-MOF was fitted into two peaks, corresponding to Ni $2p_{3/2}$ and Ni $2p_{1/2}$.

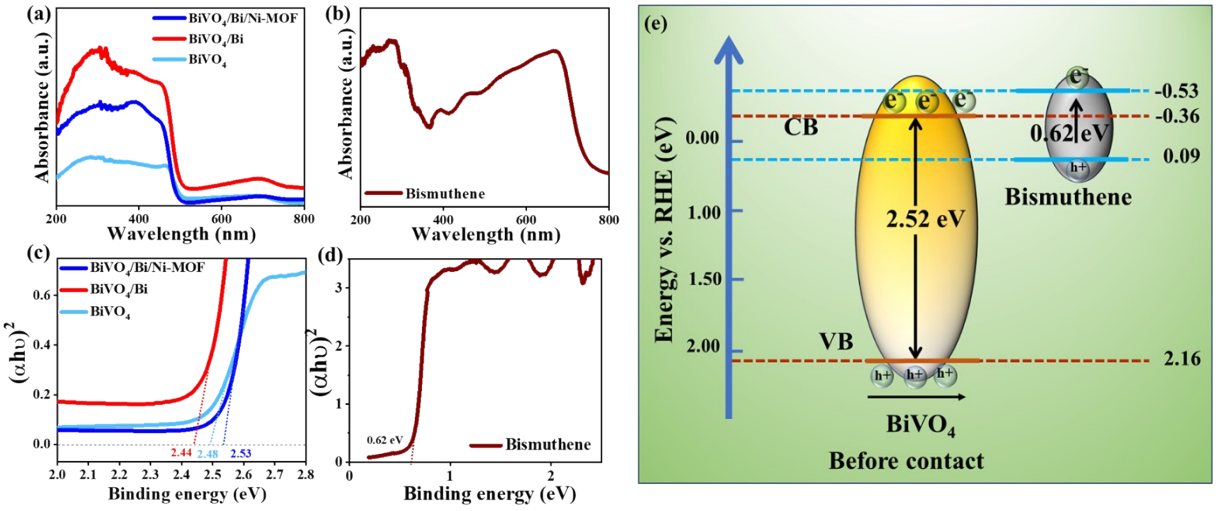

Figure S6. (a) UV-Vis spectra of $BiVO_4$, $BiVO_4$/Bi, and $BiVO_4$/Bi/Ni-MOF photoanodes. (b) UV-Vis spectrum of bismuthene, (c) Tauc plots of $BiVO_4$, $BiVO_4$/Bi, and $BiVO_4$/Bi/Ni-MOF revealing the band gap to be 2.48 eV, 2.44 eV, and 2.53 eV, respectively, (d) Tauc plot showing the band gap of bismuthene to be 0.62 eV, (e) Band alignment in $BiVO_4$ and bismuthene.

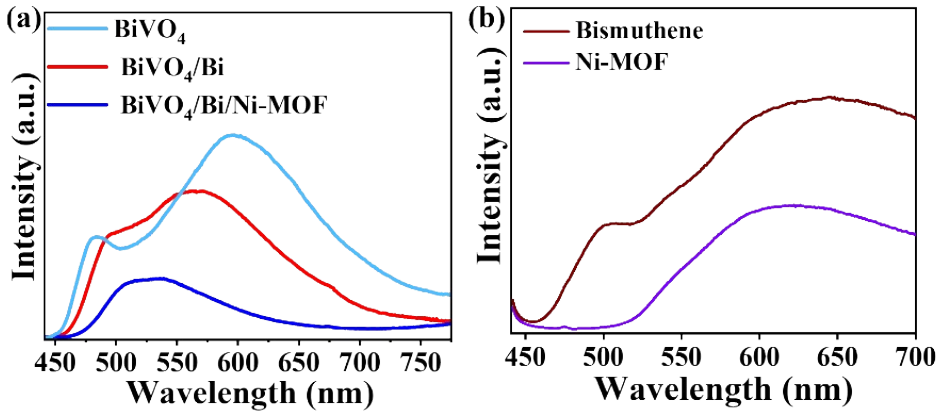

Figure S7. (a-b) PL emission spectra of $BiVO_4$, and modified photoanodes. $BiVO_4$ emits at 480 nm and 590 nm, while $BiVO_4$/Bi/Ni-MOF shows emission peaks at 510 nm and 538 nm. The shift in the two fluorescence peaks in $BiVO_4$ and $BiVO_4$/Bi/Ni-MOF compared to the $BiVO_4$/Bi and $BiVO_4$/Ni-MOF can be explained by the charge transfer from $BiVO_4$ to Ni-MOF. A significant change in the emission peak λ_{max} was observed by the loading of bismuthene and Ni-MOF on $BiVO_4$ because of the strong electronic interaction between the components.

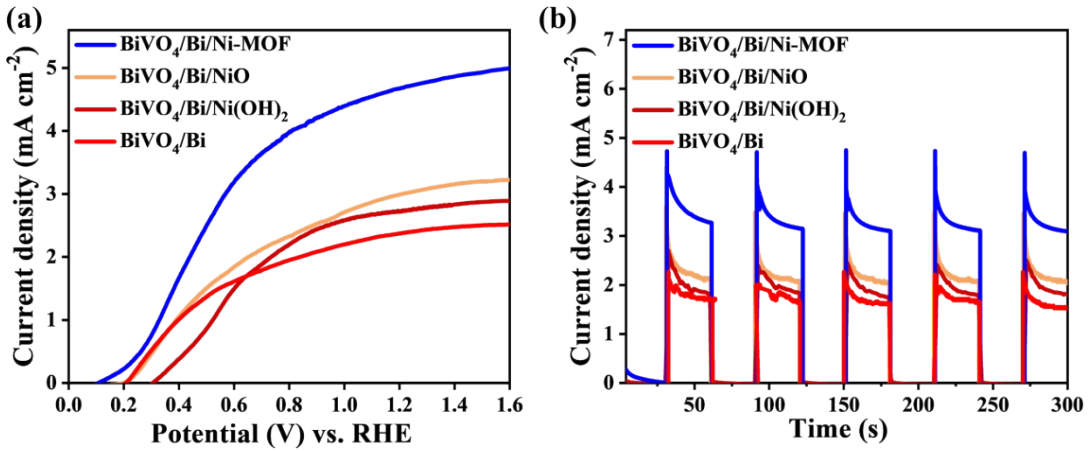

Figure S8. (a) LSV profiles of $BiVO_4$/Bi photoanodes modified with Ni-based cocatalysts (NiO, $Ni(OH)_2$, and Ni-MOF) in phosphate buffer in the presence of light. (b) Photocurrent of all $BiVO_4$/Bi/Ni-Based (NiO, $Ni(OH)_2$, and Ni-MOF) at 1.23 V vs. RHE. While $BiVO_4$/Bi/NiO and $BiVO_4$/Bi/$Ni(OH)_2$ improve PEC activity compared to bare $BiVO_4$/Bi, $BiVO_4$/Bi/Ni-MOF delivers the highest activity, highlighting the role of MOF as a cocatalyst.

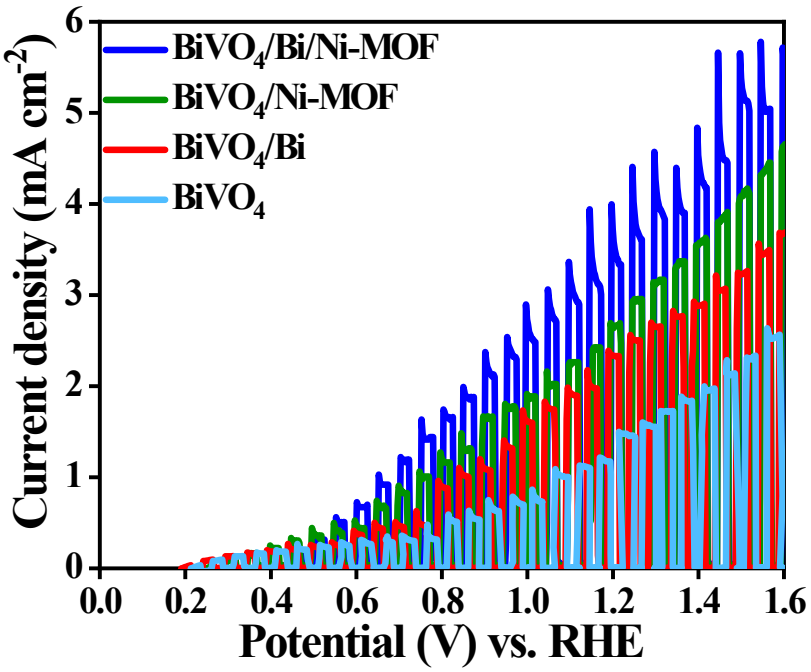

Figure S9. Photocurrent density-voltage curves of all the photoanodes with chopped illumination.

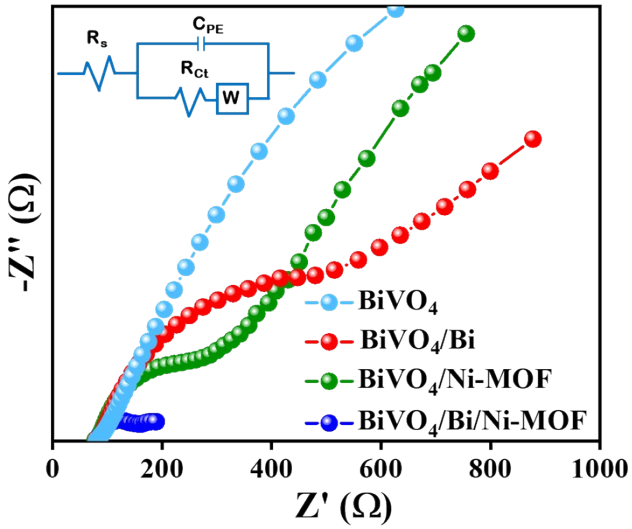

Figure S10. EIS of all photoanodes in the presence of light.

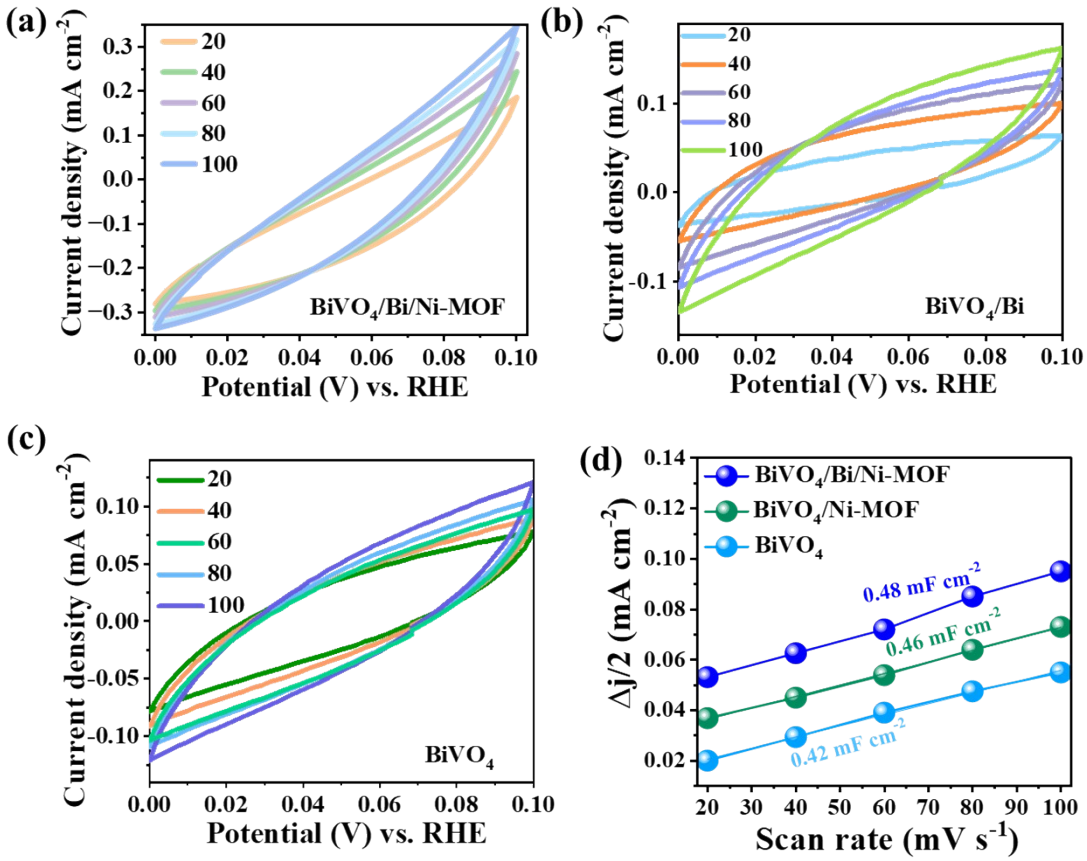

Figure S11. Electrochemical capacitive current in the non-faradaic potential range of 0 V to 0.1 V vs. RHE, used to determine the double-layer capacitance (C_{dl}) of (a) $BiVO_4$/Bi/Ni-MOF, (b) $BiVO_4$/Bi, and (c) $BiVO_4$ in the dark, (d) plots for the determination of C_{dl}.

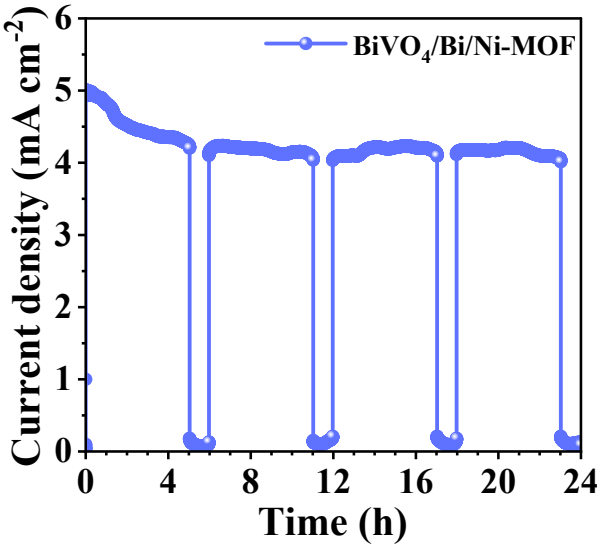

Figure S12. Chronoamperometry study of $BiVO_4$/Bi/Ni-MOF photoanode under illumination and dark at 1.23 V vs. RHE (5 h light, 1 h dark).

Table S2. Comparison of photoelectrochemical activity of different $BiVO_4$-based photoanodes.

Photoanode	Cocatalyst	Current density ($mA\ cm^{-2}$) @ 1.23 V_{RHE}	ABPE (%)	IPCE (%)	Ref.
$BiVO_4$/Bi	**Ni-MOF**	**4.76**	**2.01% @ 0.59 V_{RHE}**	**62% @ 420 nm**	**This work**
$BiVO_4$	**Ni-MOF**	**2.77**	**1.48% @ 0.58 V_{RHE}**	**49% @ 420 nm**	**This work**
$BiVO_4$	5% Rh:$SrTiO_3$	0.8	-	12% @ 450 nm	5
$BiVO_4$	FeO_x	1.1	-	21% @ 380 nm	6
$BiVO_4$	CoMnZn-LDH	1.1	0.27% @ 0.21 V_{RHE}	58%@380 nm	7
$BiVO_4$	CoPi	1.1	-		8
$BiVO_4$	NiO_x	0.5	-	43% @ 450 nm	9
W:$BiVO_4$	CoPi	1.5	-	42% @ 420 nm	10
V_2O_5/$BiVO_4$	NiOOH	1.2	-	21% @ 425 nm	11
Fe_2O_3/$BiVO_4$	NiFe-LDH	1.7	-	35% @ 400 nm	12
W:$BiVO_4$	Ni-bicarbonate	2.1	-	44% @ 440 nm	13
$BiVO_4$	FeOOH	2.1	-	-	14
$BiVO_4$	$Co_2N_{0.67}$	2.2	-	50% @ 450 nm	15
$BiVO_4$/BiOBr	-	2.69	0.26% @ 0.58 V_{RHE}	51% @ 340 nm	16
$BiVO_4$	CoPi	2.3	-	-	17
$BiVO_4$	$La_{0.2}Co_{0.2}Ce_{0.6}O_x$	2.4	-	-	18
$BiVO_4$/CdS	NiCo-LDH	2.7	1.24% @ 0.62 V_{RHE}	35.89% @ 420 nm	19
$BiVO_4$/TiO_2	IrCOOH	2.8	-	58% @ 460 nm	20
$BiVO_4$	$MnCo_2O_4$	2.8	1.1% @ 0.7 V_{RHE}	25.6% @ 460 nm	21
Zr:$BiVO_4$	AgNiOH Pi	3.2	-	42% @ 460 nm	22
$BiVO_4$	$LaFe_{0.5}Co_{0.5}O_3$	3.2	-	-	23
$BiVO_4$	CuMTZ	3.32	1.04% @ V_{RHE}	92% @ 400 nm	24
$BiVO_4$	2D $Ti_3C_2T_x$ flakes	3.5	0.78% @ 0.87 V_{RHE}	58% @ 430 nm	25
$BiVO_4$	Co-salophen	3.9	1.09% @ 0.7 V_{RHE}	89%@430 nm	26
$BiVO_4$/Black P	NiOOH	4.3	-	-	27
Borate-$BiVO_4$	NiFeV LDH	4.6	1.85% @ 0.62 V_{RHE}	80%@ 380 nm	28
$BiVO_4$	$FeCoO_x$	4.8	1.16% @ 0.84 V_{RHE}	86% @ 460 nm	29
$BiVO_4$/SnO_x	Co_4O_4/partially oxidized graphene	5.9	2.3% @ 0.6 V_{RHE}	30% @ 460 nm	30
$BiVO_4$/C_3N_4	FeOOH	5.89	2.48% @ 0.6 V_{RHE}	85% @ 460nm	31
BVO/$BiVO_4$	$NiFeO_x$	3.40	2.0% @ 0.7 V_{RHE}	60% @ 470 nm	32
$BiVO_4$/Sn:WO_3	$NiMoO_4$	2.06	0.52% @ 0.8 V_{RHE}	38.3% @ 450nm	33

References

1. K. H. Ye, H. Li, D. Huang, S. Xiao, W. Qiu, M. Li, Y. Hu, W. Mai, H. Ji and S. Yang *Nat. Commun.*, 2019, **10**, 3687.
2. L. Bai, W. Yi, J. Chen, B. Wang, Y. Tian, P. Zhang, X. Cheng, J. Si, X. Hou and J. Hou, *ACS Appl. Mater. Interfaces,* 2022, **14**, 25050–25064.
3. A. Yadav, T. Ansari, P. Mannu, B. Singh, A. K. Singh, Y. C. Huang, V. Kumar, S. Singh, C. L. Dong and A. Indra, *J. Mater. Chem. A,* 2024*,* **12**, 29072–29080.
4. T.Wang, K. Song, H. Liu, H. Li, Y. Zhang, W. Ren, R. Zhang, K. Li, F. Hen, Z. Qin and H. Hou, *J. Chem. Eng*, 2025, **509**, 161333.
5. Y. Zhang, Y. Li, D. Ni, Z. Chen and X. Wang, *Adv. Funct. Mater.* 2019, **29**, 1902101.
6. H. Saada, R. Abdallah, B. Fabre, D. Floner, S. Fryars, A. Vacher, V. Dorcet, C. Meriadec, S A. -Girard and G. Loget, *ChemElectroChem,* 2019**, 6**, 613-617.
7. T. G. Vo, Y. Taia, and C.Y. Chiang, *J. Catal.,* 2019, **370**, 1-10.
8. K. Nie, S. Kashtanov, Y. Wei, Y. S. Liu, H. Zhang, M. Kapilashrami, Y. Ye, P.-A. Glans, J. Zhong, L. Vayssieres, X. Sun and J. Guo, *Nano Energy,* 2018, **53**, 483-491.
9. L. Yongqi and J. Messinger, *Phys. Chem. Chem. Phys.,* 2014, **16**, 12014-12020.
10. D. K. Zhong, S. Choi, Daniel and R. Gamelin, *J. Am. Chem. Soc.* 2011, **133**, 45, 18370–18377.
11. A. Maheswari, K. S. Ahn and S. H. Kang. *Int. J. Hydrog. Energy*, 2019, **44**,10, 4656-4663.
12. S. Baia, H. Chua, X. Xianga, R. Luoa, J. Hea and A. Chen, *Chem. Eng. J,* 2018, **350**, 148-156.
13. S. K. Pilli, K. Summers and D. Chidambaram, *RSC Adv.,* 2015, **5**, 47080–47089.
14. S. L. Chen, L.Y. Lin, and Y. S. Chen, *Electrochim. Acta*, 2019, **295**, 507-513.
15. X. Wan, J. Su and L. Guo, *Eur. J. Inorg. Chem.* 2018*,* **22***,* 2557–2563.
16. L. Shuai, L. Tian, X. Huang, J. Dou, J. Yu and X. Chen, *Int. J. Hydrogen Energy*, 2024, **88**, 19–28.
17. Y. Ma, A. Kafizas, S. R. Pendlebury, F. Le Formal and J. R. Durran, *Adv. Funct. Mater.,* 2016*,* **26***,* 4951–4960.
18. D. Guevarra, A. Shinde, S. K. Suram, I. D. Sharp, F. M. Toma, J. A. Haber and J. M. Gregoire, *Energy Environ. Sci.*, 2016, **9**, 565—580.
19. S. Bai, Q. Li, J. Han, X. Yang, X. Shu, J. Sun, L. Sun, R. Luo, D. Li and A. Chen. *Int. J. Hydrog. Energy,* 2019*,* **44**, 45, 24642-24652.
20. M. Kan, D. Xue, A. Jia, X. Qian, D. Yue, J. Jia and Y. Zhao, *Appl. Catal. B*, 2018, **225**, 504-511.
21. D. Xu, T. Xia, H. Xu, W. Fan and W. Shi, *Chem. Eng. J.,* 2020, **392**, 124838.
22. M. N. Shaddad, P. Arunachalam, A. A. Alothman, A. M. Beagan, M. N. Alshalwi and A. M. A. Mayouf, *J. Catal.*, 2019, **371**, 10-19.
23. Y. Gao, G. Yan, Y. Dai, X. Li, J. Gao, N. Li, P. Qiu and L. Ge, *ACS Appl. Mater. Interfaces*, 2020, **12**, 15, 17364–17375.
24. J. -W. Ji, L. -J. Zhang, H. -C. Wang, Y. -X. Duan, X. -Z. Yue, J.-H. Chen and S. -S. Yi, *Chem. Eng. J.,* 2024, 484, 149597.
25. D. Yan, X. Fu, Z. Shang, J. Liu and He. Luo, *J. Chem. Eng.*, 2019, **361**, 853-861.

26. Y. Liu, Y. Jiang, F. Li, F. Yu, W. Jianga and L. Xia, *J. Mater. Chem. A,* 2018, **6**,10761–10768.
27. K. Zhang, B. Jin, C. Park, Y. Cho, X. Song, X. Shi, S. Zhang1, W. Kim, H. Zeng, and J. H. Park, *Nat. Commun.*, 2019, **10**, 2001.
28. Q. Meng, B. Zhang, H. Yang, C. Liu, Y. Li, A. Kravchenko, B. Zhang, H. Yang, C. Liu, Y. Li, X. Sheng, L. Fan and L. Sun, *Mater. Adv*., 2021, **2**, 4323-4332.
29. S.Wang, T. He, J. H. Yun, Y. Hu, M. Xiao, M. Xiao, A. Du and L. Wang, *Adv. Funct. Mater*. 2018, **28**, 1802685.
30. S. Ye, W. Shi, Y. Liu, D. Li, H. Yin, H. Chi, Y. Luo, N. Ta, F. Fan, X. Wang, and C. Li, *J. Am. Chem. Soc.,* 2021, **143**, 12499–12508.
31. S. Xia, F. Xu and B. Weng*, J. Mater. Chem. A*, 2024, **12**, 4635–4642.
32. Z. Xie, D. Chen, J. Zhai, Y. Huang and H. Ji, *Appl. Catal. B*, 2023, **334**, 122865.
33. H. T. Htet, Y. Jung, Y. Kim and S. Lee, *ACS Appl. Mater. Interfaces*, 2024, **16**, 52383–52392.